ELSEVIER

Journal of Nuclear Materials 247 (1997) 138–146

journal of nuclear materials

Effect of external restraint on bubble swelling in UO_2 fuels

S. Kashibe *, K. Une

Nippon Nuclear Fuel Development Co., Ltd., 2163, Narita-cho, Oarai-machi, Higashi Ibaraki-gun, Ibaraki-ken 311-13, Japan

Abstract

The effect of external restraint on bubble growth in unirradiated UO_2 fuels has been examined using a high temperature and high pressure furnace. The powder compacts of UO_2 were sintered at 1800°C in high pressure Ar/0.2% H_2 mixed gas of 50 or 100 MPa, and then the sintered pellets were annealed at lower ambient pressures than the sintering pressures. This treatment caused bubbles in the pellets becoming overpressurized; the excess pressure driving force caused bubble growth. The growth rate significantly depended on the magnitude of the driving force, and the growth of high pressure bubbles was effectively suppressed by very strong external restraints even at the high annealing temperatures of 1600–1800°C. The bubble growth data obtained under various excess pressures and annealing temperatures were analyzed by using a well known model for bubble growth rate, in which the grain boundary diffusion coefficient was best-fitted based on the data. The bubble size calculated by the above model was in good agreement with the obtained data unless the swelling exceeded about 8%. Above this value, the measured swelling was saturated, due to interlinking of grown bubbles and subsequent gas release. © 1997 Elsevier Science B.V.

1. Introduction

Fission gas atoms generated in the UO_2 lattice have a strong tendency to precipitate into intra- and intergranular bubbles, because of their low solubility. At higher burnups, larger amounts of fission gases diffuse into the bubbles, which thereby become overpressurized or exist in a non-equilibrium state. During steady state and transient conditions, the flux of vacancies flows into the overpressurized bubbles driven by their excess pressure, which eventually causes fuel swelling. This swelling is one of the most important clad-straining mechanisms at high burnups. From the large difference between grain boundary and lattice diffusivities of vacancies, intergranular bubble swelling is generally more important than intragranular bubble swelling [1,2]. However, at higher burnups above 44 GWd/t, the latter contribution gradually increases, and becomes almost equivalent to, or larger than, the former contribution, mainly due to formation of the subdivided grain structure [3]. The grain boundary bubbles also play an important role in the course of fission gas release from fuel pellets, since grain edge tunnel formation due to the interconnection of intergranular bubbles is a major release path.

Therefore, in order to evaluate fission gas behavior at high burnups by a fuel performance code, a sophisticated model based on physical mechanisms of bubble growth and fission gas release is essential. In the model, the effect of PCI or external restraint has to be taken into consideration. In some irradiation tests [4–6], bubble growth and fission gas release have been greatly affected by external restraints. An isothermal irradiation test carried out by Zimmermann [4] revealed that compressive load significantly reduced fission gas swelling, i.e., to about half of unrestrained swelling at higher temperatures of 1600–1900 K. Kogai et al. [5] and Mogensen et al. [6] emphasize the importance of mechanical restraint pressure in fission gas release behavior during power bump tests; in the fuel rods accompanying an intense PCI, fission gas release was retarded at high power level, due to the prevention of bubble interlinkage on the grain boundaries. Then, when the power was decreased, the restraint pressure was removed with the result that grain boundary bubbles were able to interlink allowing the trapped gas to escape. In the latter paper [6], in fact, the bubble swelling was considerably suppressed.

* Corresponding author. Tel.: +81-29 266 2131; fax: +81-29 266 2589; e-mail: kashibe@nfd.co.jp.

0022-3115/97/$17.00
PII S0022-3115(97)00083-4

Irradiation tests, however, often include unknown and uncontrollable temperature, time and irradiation histories. Furthermore, it is difficult to estimate accurately external restraint force and gas pressure in the bubbles, which are both essential to the verification of the basic fission gas model. From this viewpoint, the out-of-pile simulation technique for bubble swelling is very attractive. Une [7] caused fuel swelling by generating CO/CO_2 gas bubbles. Schrire [8] reproduced it by annealing unirradiated UO_2 pellets at ambient pressure, which had been sintered in high pressure Ar. The latter technique is much simpler than carrying out an irradiation test, since bubble growth is caused solely by known excess pressure driving forces under isothermal conditions without irradiation and gas production during the growth.

In the present study, the effect of external restraint on bubble growth has been systematically examined for unirradiated UO_2 pellets by using a high temperature and high pressure furnace for wide ranges of temperature and excess pressure. The kinematic data of bubble growth and swelling were evaluated by a well-known bubble growth model [9], and the best-fitted grain boundary diffusion coefficients were derived.

2. Experimental

2.1. Apparatus

Bubble swelling experiments of UO_2 pellets were carried out in a high temperature and high pressure furnace which was installed in a shielded glove box. The furnace has a controlling system for temperature and pressure, and it is capable of operation at temperatures up to 2000°C and pressures up to 200 MPa. The maximum heating rate was 1500°C. There is also a measuring system for ^{85}Kr released from the irradiated pellets. Fig. 1 gives a schematic diagram of the high pressure furnace and measuring system of released ^{85}Kr. The fuel specimens were heated by the graphite heater located inside of a thermal insulation hood.

The temperature was measured by a thermocouple installed near the heater. High pressures in the furnace were achieved by a high purity mixed gas of Ar/0.2% H_2 compressed with a mechanical pump. The pressure was measured by a pressure gauge of the strain gauge type. Pressure control to stabilize the pressure changes caused by thermal expansion of gas was carried out by releasing the gas in the furnace with an on/off-type valve controlled by the pressure gauge. The respective accuracies for pressure and temperature control were below $\pm 1\%$ and $\pm 5\%$ for the set value.

A sampling line was provided for measuring ^{85}Kr activities released from irradiated specimens into the high pressure gas. The sampled gas was led from the sampling tube, located near the graphite heater, to an evacuated ionization chamber. Evacuating the ionization chamber and sampling the highly compressed gas were carried out automatically. The concentration of water vapor in the compressed gas was monitored by a dew-point meter connecting to the ionization chamber. When using dry Ar/0.2% H_2 mixed gas, the dew point during sintering and annealing tests was confirmed to be a sufficiently low value of -36°C.

2.2. Swelling experiment

The UO_2 pellets containing high pressure as-sintered bubbles were obtained by sintering unirradiated powder

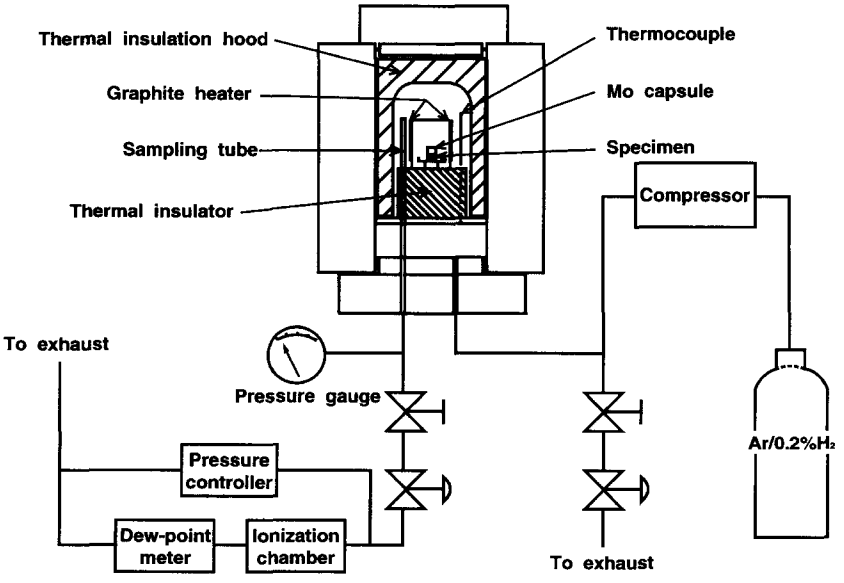

Fig. 1. Schematic diagram of furnace chamber and ^{85}Kr measuring system.

compacts under a high pressure condition. The UO_2 powder (O/U ratio 2.06; specific surface area 4.2 m^2/g) was pressed into compacts of 7 mm diameter and 7.2 mm height, and their density was about 52% TD. An Mo capsule containing the UO_2 compacts was loaded into the high pressure furnace. After the atmosphere in the furnace had been sufficiently flushed several times with the Ar/0.2% H_2 mixed gas, the internal pressure was increased to 50 or 100 MPa. The pressure was kept while heating the furnace to 1800°C at the rate of 350°C/h, holding it at 1800°C for 1 h, and then cooling it to room temperature at the rate of 1500°C/h. The density of the sintered pellets was measured by the immersion method. Mean grain size and bubble size were obtained by image analysis based on scanning electron micrographs of etched and polished surfaces of specimens. The values obtained for the sintered pellets were 90.7 ± 0.6% TD, 3.0 ± 0.2 μm mean grain size and 0.62 ± 0.1 μm mean bubble size. Grain size and pore size were given as three-dimensional values, which were obtained by multiplying the two-dimensional values by 1.5 [10].

These high pressure sintered pellets were then annealed at lower temperatures of 1300–1800°C and lower ambient pressures of 10–90 MPa than the sintering temperature and pressure for durations of 10 min–5 h to obtain bubble growth and swelling transient data.

3. Bubble growth model

Assuming that the bubble growth is rate-controlled by the grain boundary diffusion of cations and that the bubbles have an initial array of equally spaced grain faces, the model of Hull and Rimmer [9] can be applied. Their equation for the growth rate of bubble radius, r, is expressed as

$$dr/dt = 2\pi D_g a \Omega (\Delta P - 2\gamma/r)/(kTsr), \quad (1)$$

with $\Delta P = P - p$, where P is the internal gas pressure in the bubble, p is the external hydrostatic pressure, D_g is the grain boundary diffusion coefficient of cations, a is the grain boundary width, Ω is the atomic volume, γ is the surface energy, s is the mean inter-bubble spacing, k is the Boltzmann constant and T isthe absolute temperature.

The bubble growth rate is proportional to the excess pressure driving force $(\Delta P - 2\gamma/r)$ of the bubble and cation diffusivity.

The present UO_2 pellets were sintered in the high pressure Ar/0.2% H_2 mixed gas of 50 or 100 MPa at 1800°C for 1 h. Therefore they have many high pressure bubbles on the grain boundaries. When annealing the pellets at lower temperatures and lower ambient pressures than the sintering conditions, the bubbles in the pellets become overpressurized, and the excess driving force causes bubble growth. In the present out-of-pile experiments, the excess pressure and temperature could be controlled accurately. Hence, the validity of the rate equation and the appropriate values of grain boundary diffusion coefficients of cations could be examined.

4. Results

4.1. Swelling

The swelling data were evaluated from pellet densities before and after annealing tests, as measured by the im-

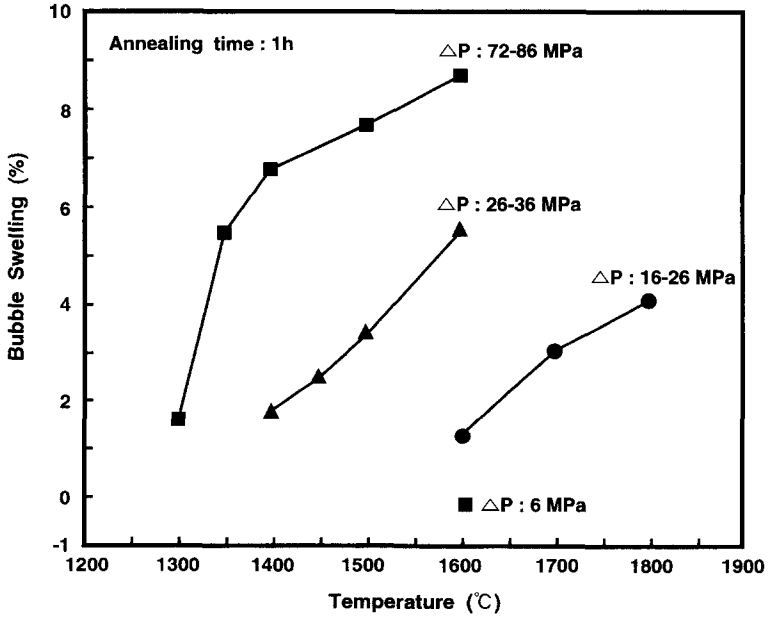

Fig. 2. Relation between bubble swelling and temperature.

mersion method. Fig. 2 shows the relation between bubble swelling and annealing temperature of the pellets sintered in 100 MPa Ar/0.2% H_2 gas at 1800°C for 1 h. The internal pressure in the as-sintered bubble of 0.62 μm at 1800°C is equal to 100 MPa plus the equilibrium pressure ($2\gamma/r$) of 6 MPa. The annealing was conducted for 1 h at temperatures from 1300 up to 1800°C lower temperatures than the sintering temperature. In this experimental series, four runs were carried out at different external pressures of 10, 60, 80 and 90 MPa, to examine the effect of external restraint pressure. Each run has a small range of excess pressure, ΔP, since the bubble internal pressure varies with annealing temperature. Eventually, the swelling data are summarized in terms of four different levels of ΔP: high, 72–86 MPa; upper middle, 26–36 MPa; lower middle, 16–26 MPa; and low, 6 MPa. The lowest ΔP level corresponds to the strongest external restraint condition, and the highest ΔP level is the weakest.

The obtained swelling data in Fig. 2 distinctly demonstrate the importance of ΔP, or external restraint pressure, as well as annealing temperature. Naturally the swelling increases with higher annealing temperature at the same external pressure. When comparing the data at a given annealing temperature, larger values of swelling are observed at larger ΔP, i.e., smaller external restraint levels. The swelling is about 6–7% under an external pressure of 10 MPa (ΔP 72–86 MPa) at lower temperatures of 1350–1400°C, while it is only about 3–4% under an external pressure of 80 MPa (ΔP 16–26 MPa) even at higher temperatures of 1700–1800°C. For the case of the highest external pressure of 90 MPa at 1600°C, in which the external excess driving force of $\Delta P - 2\gamma/r$ becomes nearly zero, no swelling is observed. In an isothermal irradiation test, Zimmermann [4] found that compressive loads of 2–50 MPa reduced fission gas swelling to about half of the unrestrained swelling at higher temperatures of 1600–1900 K. The onset temperature for measurable bubble swelling shifts to the higher temperature side when the external restraint pressure is increased (or the value of ΔP is decreased). This phenomenon qualitatively agrees with the finding that the burst release temperature of fission gas becomes lower with increasing burnup in post-irradiation annealing experiments under a non-external restraint condition [11]. Namely, higher internal pressures in the bubbles at higher burnups lead to their faster growth rates, thereby interlinking bubbles to form grain boundary tunnels at lower temperature. The fission gases accumulated in the grain boundaries can be released rapidly through the tunnels.

The swelling transient curves obtained at constant temperatures of 1350, 1450 and 1700°C with ΔP of 21–73 MPa are given in Fig. 3. The sintering pressure of the pellets was 100 MPa, except for the case of $\Delta P = 37$ MPa and $T = 1450$°C for which it was 50 MPa. The swelling values show a steep increase during an initial annealing stage of within 1 h, followed by a gradual increase of swelling. Finally, they saturate at about 3–10% after 1–3 h annealing, with significant dependence on the magnitude of ΔP. The lower saturation values of 3–4%, which were obtained at the two conditions of $\Delta P = 21$ MPa at $T = 1700$°C and $\Delta P = 28$ MPa at $T = 1450$°C, are attributed to a decline and disappearance of the excess pressure driving force for bubble growth. The higher saturation swelling values of 8–10% obtained at the conditions of $\Delta P = 37$

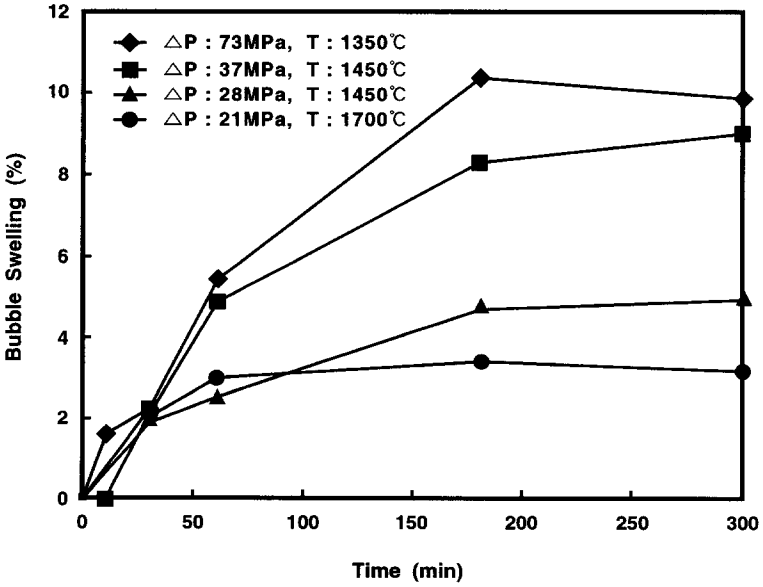

Fig. 3. Bubble swelling transient curves.

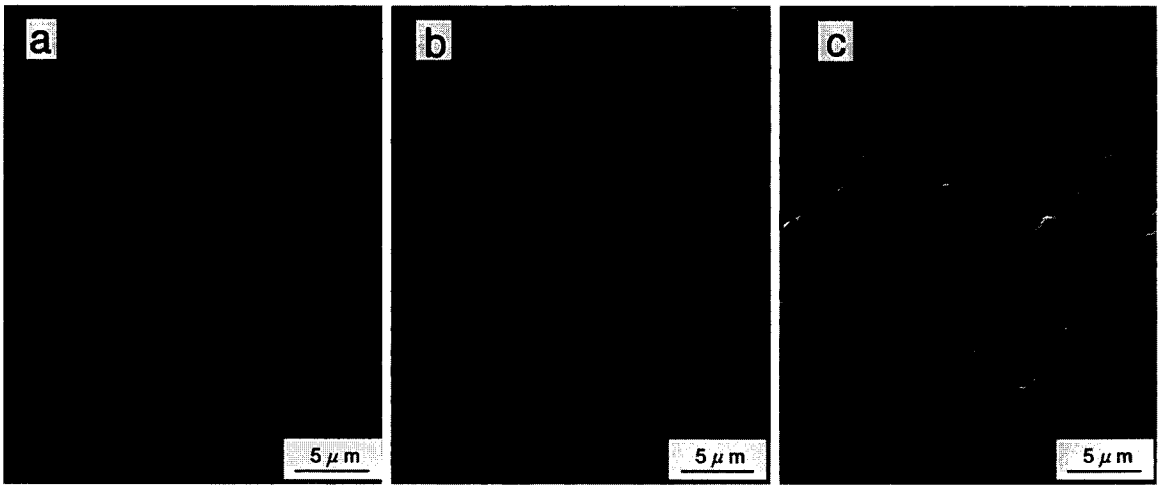

Fig. 4. Scanning electron micrographs of polished surface of specimens: (a) before annealing, (b) after 1600°C × 1 h annealing at $\Delta P = 86$ MPa, (c) after 1600°C × 1 h annealing at $\Delta P = 16$ MPa.

MPa at $T = 1450$°C and $\Delta P = 73$ MPa at $T = 1350$°C, are mainly caused by gas release due to bubble coalescence and interlinkage. In fact, bubble interlinkage was clearly observed, as shown in the next section.

For the bubble radius, r, and grain diameter, d, the theoretical saturated porosity A_{sat} at which the grain face bubbles begin to link with each other can be given by Eq. (2) [7]:

$$A_{sat} = \pi r W / d, \tag{2}$$

where W is the volume correction factor of a lenticular bubble, depending on the dihedral angle. For the measured mean radius of $r = 0.46$ μm and grain diameter of $d = 3.0$ μm of the specimen annealed at $\Delta P = 73$ MPa and $T = 1350$°C, the theoretical saturated swelling is calculated to range from 20–40% for the cases of $W = 0.44$ (lenticular bubble) and 1.0 (spherical bubble). When considering that fission gas release occurs sufficiently under the condition of smaller fractional grain face coverages of the bubbles (40–50%), compared to the theoretical value of 79% for the bubble interlinkage condition [12], it is reasonable to expect that gas release begins around the total porosities of

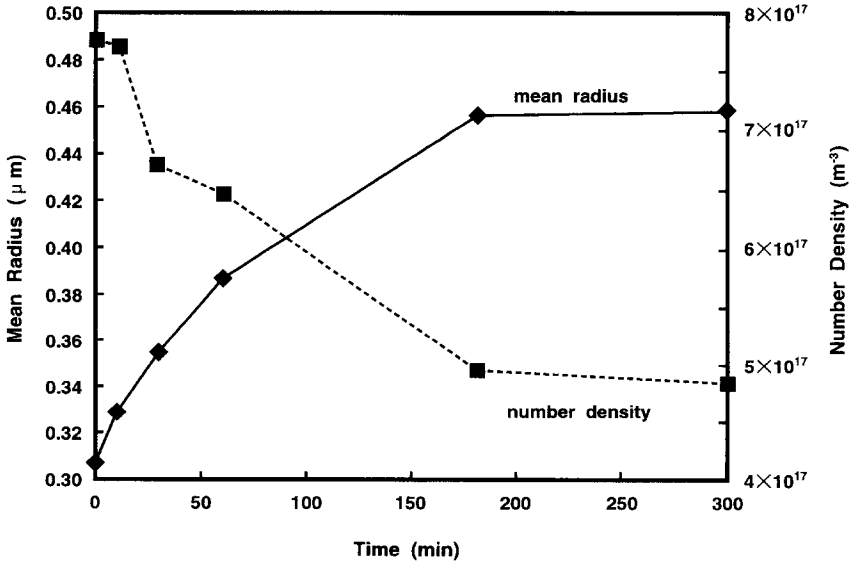

Fig. 5. Time dependence of mean bubble radius and number density before and after annealing in $\Delta P = 73$ MPa at 1350°C.

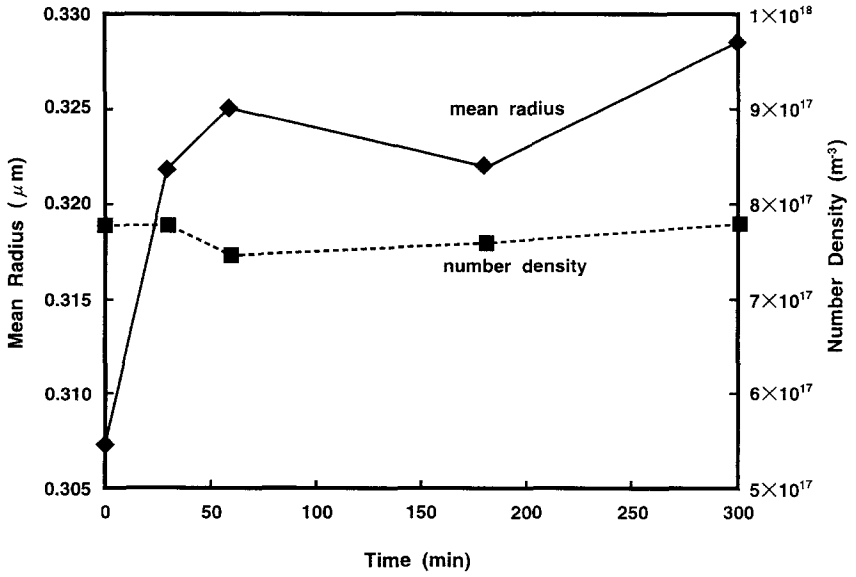

Fig. 6. Time dependence of mean bubble radius and number density before and after annealing in $\Delta P = 21$ MPa at 1700°C.

17–19% (bubble swelling 8–10%) obtained in the present experiments.

4.2. Bubble morphology

Scanning electron micrographs of the polished surface of specimens before and after the annealing experiments (1600°C for 1 h) for ΔP of 86 and 16 MPa are given in Fig. 4. In the as-sintered specimen, there is a high density of small bubbles of about 0.5 μm size on the grain boundaries. Furthermore, sparse, large bubbles of a few μm size appear at corners of grains. In the specimen annealed with ΔP of 86 MPa, the small intergranular bubbles have clearly become larger, and coalesced and interlinked large bubbles are found. The high pressure gas enclosed in the bubbles has possibly escaped through the partially interlinked bubbles. For the smaller ΔP of 16 MPa, bubbles grown in this way are few in number. Thus, growth of bubbles is strongly suppressed by loading of the strong external restraint.

The observed time dependencies of mean bubble radius and number density before and after annealing at 1350°C for the largest ΔP of 73 MPa are shown in Fig. 5. The bubble radius increases with time from 0.31 μm to 0.46 μm during a 3 h annealing, and after that it is almost saturated. This tendency is fully consistent with the swelling curve shown in Fig. 3. In contrast to bubble size, the bubble number density decreases with time, dropping from 8×10^{17} m^{-3} to 5×10^{17} m^{-3} after a 3 h annealing and is almost saturated. These quantitative data also support the occurrence of bubble coalescence. For the specimens annealed at 1700°C with the smaller ΔP of 21 MPa, the corresponding data are shown in Fig. 6. The bubble radius rapidly increases within a 1 h annealing from 0.31 μm to 0.32–0.33 μm. On the other hand, the bubble number density is almost constant at 8×10^{17} m^{-3}, irrespective of annealing time. This clearly indicates that no interlinkage of bubbles occurred for the latter case.

5. Discussion

From the present data of simulated bubble swelling, the validity of the bubble growth rate equation reported by Hull and Rimmer [9] has been proved. Hence an important rate constant, the grain boundary diffusion coefficient of cations, can be derived by analyzing bubble growth data of Figs. 5 and 6. For the evaluation for the data of Fig. 5 ($\Delta P = 73$ MPa, $T = 1350$°C), the effect of bubble coalescence must be taken into consideration, since the time dependencies of the mean radius and number density measured by the present experiments show the bubble coalescence.

First of all, when considering that two bubbles with the same radius r_1 coalesce and become one bubble with radius r_2, and that the total bubble volume does not change before and after the bubble coalescence, r_2 is given by Eq. (3):

$$r_2 = 2^{1/3} r_1. \tag{3}$$

This just-coalesced bubble has a newly generated overpressure because the bubble pressure is the same as that in the

original two bubbles, therefore the coalesced bubble swells to radius r_3. This bubble radius r_3 is given by Eq. (4) [13]:

$$r_3 = 2^{1/2} r_1. \tag{4}$$

The bubble radius r^* after coalescing of the bubble falls in the range of $2^{1/2} r_1 \geqslant r^* \geqslant 2^{1/3} r_1$. Thus, the corrected radius of a non-coalesced bubble was estimated by subtracting the evaluated influence of the bubble coalescence from the measured values of the bubble radius and number density. The total bubble volume in the unit volume of a pellet, calculated from the measured bubble radius r_M and number density N_M, is equal to the total bubble volume of the non-coalesced and coalesced bubbles. This is shown in Eq. (5):

$$r_M^3 N_M = r_c^3 N_{M0}(1 - C) + (Jr_c)^3 C N_{M0}/2, \tag{5}$$

where C is the bubble coalescence probability given by $C = 2(N_{M0} - N_M)/N_{M0}$, N_{M0} is the initial bubble number density before annealing, r_c is radius of the non-coalesced bubble, J is a factor depending on whether the bubble grows due to the newly generated overpressure or not, which is taken from Eqs. (3) and (4) within the range of $2^{1/2}$–$2^{1/3}$. Thus the value of r_c is given by

$$r_c = \left(N_M / \left(N_{M0}\left(1 - C + J^3 C/2\right)\right)\right)^{1/3} r_M. \tag{6}$$

Fig. 7 shows the transients of the measured bubble radii and the corrected values from Eq. (6) for the annealing case of $\Delta P = 73$ MPa and $T = 1350$°C. In addition, simply calculated bubble radii from Eq. (1) (the Hull–Rimmer model) are plotted by dashed lines in the figure. In the calculation, the values of grain boundary width $a = 5 \times 10^{-10}$ m, atomic volume $\Omega = 4 \times 10^{-29}$ m^3, and surface energy $\gamma = 1$ J/m^2 were used. The mean intergranular bubble spacing s was calculated from the initial bubble number density N_{M0} and the grain size d by using the equation of $s = (N_{M0} d/3)^{-1/2}$. The value of the grain boundary diffusion coefficient was multiplied by the correction factor F based on the values reported by Reynolds and Burton [14]. As a result, the value of the correction factor for the grain boundary diffusion coefficient is in the range of about 0.9–1.8, in which the corrected and the model calculation results agree well, except for the 5 h annealing. This difference is due to gas release based on the bubble coalescence and interlinkage. Next the data for the case of $\Delta P = 21$ MPa and $T = 1700$°C were examined by assuming the activation energy of grain boundary diffusion is 239 kJ/mol as reported by Reynolds and Burton. In this case, the above correction is not necessary, because no bubble coalescence occurred. From simulated bubble swelling experiments by Schrire [8], the value of 200 kJ/mol was obtained. A comparison between the measured and calculated results is also given in Fig. 7 and there is good agreement. Finally the grain boundary diffusion coefficients, evaluated on the basis of the present experimental data are expressed by

$$D_g = 1.9 \times 10^{-6} \exp(-239\,000/RT)\ \text{m}^2\,\text{s}^{-1}. \tag{7}$$

The obtained temperature dependence of the grain boundary diffusion coefficient is given in Fig. 8, together with the values reported by Reynolds and Burton [14] and Yajima et al. [15]. The present data are in good agreement with the Reynolds and Burton.

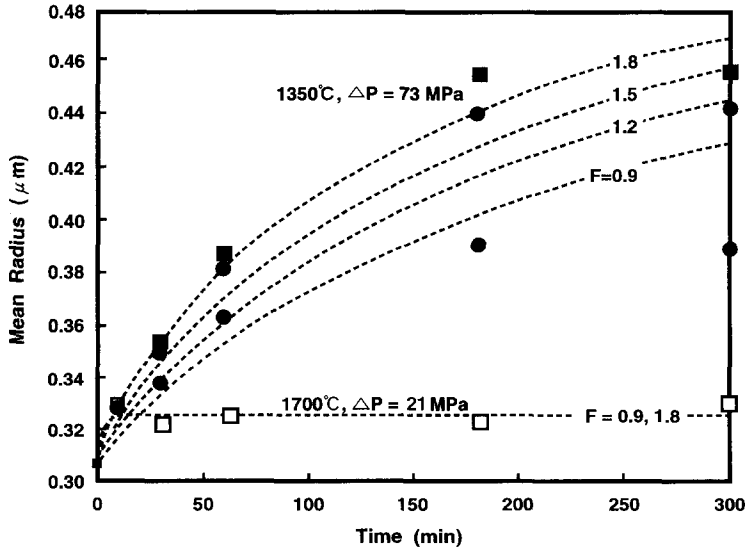

Fig. 7. Comparison between measured bubble growth and calculated values based on Hull and Rimmer model. ■,□ measured values at $\Delta P = 73$ MPa and 1350°C and at $\Delta P = 21$ MPa and 1700°C; ● measured values corrected for coalescence of bubbles at $\Delta P = 73$ MPa and 1350°C (Eq. (6)); F correction factor for D_g of Reynolds and Burton [14]; - - - calculated bubble radii from the Hull and Rimmer model.

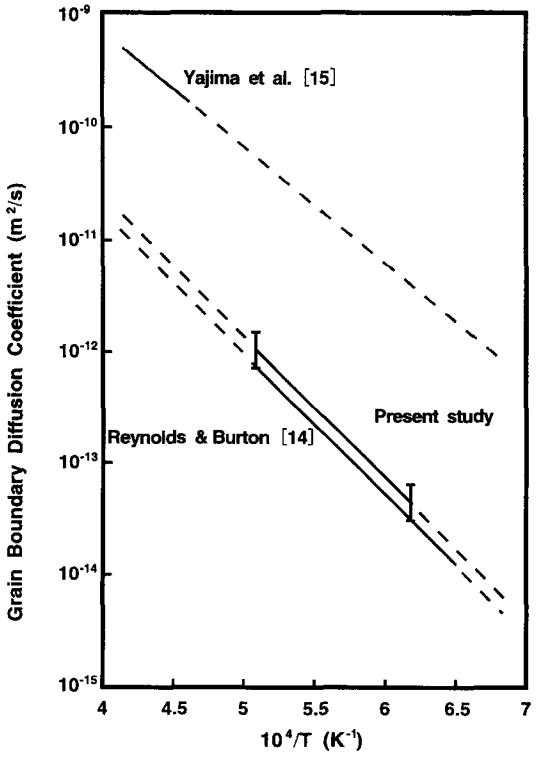

Fig. 8. Arrhenius plots of grain boundary diffusion coefficient against $1/T$.

Next by bubble swelling S was evaluated from the bubble radius calculated by the bubble growth model of Eq. (1) and the measured bubble number density N_M, by the equation

$$S = 4\pi\left(r^3 - r_0^3\right)N_M/3, \tag{8}$$

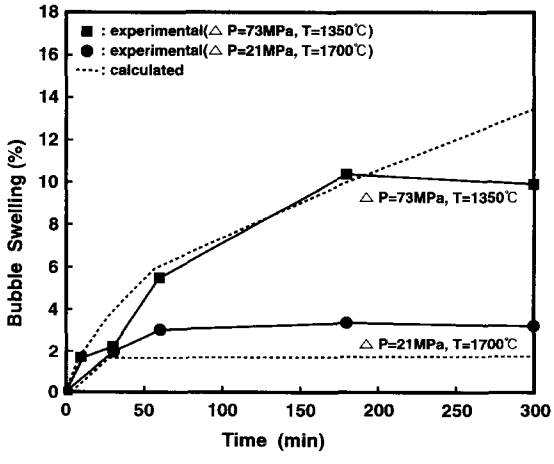

Fig. 9. Comparison between measured bubble swelling and calculated values.

where r_0 is the measured initial bubble radius. The comparison between the measured and calculated swelling values is given in Fig. 9 for the two cases of $\Delta P = 73$ MPa and $T = 1350$°C, and $\Delta P = 21$ MPa and $T = 1700$°C. For both cases the agreement is within $\pm 2\%$ swelling. The large difference with the 5 h annealing for the case of $\Delta P = 73$ MPa and $T = 1350$°C is attributed to gas release due to bubble interlinkage. For further analysis of bubble swelling, a mechanistic fission gas model incorporating bubble interlinkage and gas release is needed.

6. Conclusions

The UO_2 pellets with high pressure bubbles were prepared by sintering compacts in pressures of 50 and 100 MPa at 1800°C for about 1 h, and then annealing them at pressures of 10–90 MPa and 1350–1700°C for 10 min–5 h. The effect of external restraint on bubble swelling was examined by measuring swelling, bubble radius and bubble number density for the annealed pellets. The conclusions were as follows.

(1) Bubble swelling was reproduced by annealing unirradiated UO_2 pellets at lower ambient pressure; the pellets had been sintered in high pressure Ar/0.2% H_2 mixed gas.

(2) The onset temperature for measurable bubble swelling shifted to the higher temperature side when the external restraint pressure was increased. The growth of bubbles was strongly suppressed by loading of strong external restraint.

(3) The swelling values showed a steep increase during an initial annealing stage which was within 1 h, followed by a gradual increase of swelling. Finally, they saturated at about 3–10% after 1–3 h annealing; this depended significantly on the magnitude of ΔP. The lower saturation values of 3–4%, which were obtained at the two conditions of $\Delta P = 21$ MPa at $T = 1700$°C and $\Delta P = 28$ MPa at $T = 1450$°C; were attributed to a decline and disappearance of the excess pressure driving force for bubble growth. The higher saturation swelling values of 8–10% obtained at the conditions of $\Delta P = 37$ MPa at $T = 1450$°C and $\Delta P = 73$ MPa at $T = 1350$°C were mainly caused by gas release due to bubble coalescence and interlinkage.

(4) The grain boundary diffusion coefficients, evaluated on the basis of the present experimental data were expressed by

$$D_g = 1.9 \times 10^{-6}\exp(-239\,000/RT)\ \mathrm{m^2\,s^{-1}}.$$

The present grain boundary diffusion coefficients were in good agreement with the values reported by Reynolds and Burton.

(5) Bubble swelling was evaluated from the bubble radius calculated by the bubble growth model and the observed bubble number density for the two cases of

$\Delta P = 73$ MPa at $T = 1350$°C and $\Delta P = 21$ MPa at $T = 1700$°C. For both cases the agreement was within $\pm 2\%$ swelling from the comparison between the measured and calculated swelling values.

References

[1] R.J. White, M.O. Tucker, J. Nucl. Mater. 118 (1983) 1.
[2] M. Mogensen, C.T. Walker, I.L.F. Ray, M. Coquerelle, J. Nucl. Mater. 131 (1985) 162.
[3] S. Kashibe, K. Une, K. Nogita, J. Nucl. Mater. 206 (1993) 22.
[4] H. Zimmermann, J. Nucl. Mater. 75 (1978) 154.
[5] T. Kogai, K. Ito, Y. Iwano, J. Nucl. Mater. 158 (1988) 64.
[6] M. Mogensen, C. Bagger, C.T. Walker, J. Nucl. Mater. 199 (1993) 85.
[7] K. Une, J. Nucl. Mater. 158 (1988) 188.
[8] D.I. Schrire, DOE/ER/10591-T2 (1983).
[9] D. Hull, D.E. Rimmer, Philos. Mag. 4 (1959) 673.
[10] M.I. Mendelson, J. Am. Ceram. Soc. 52 (1969) 443.
[11] K. Une, S. Kashibe, J. Nucl. Sci. Technol. 27 (1990) 1002.
[12] S. Kashibe, K. Une, J. Nucl. Sci. Technol. 28 (1991) 1090.
[13] D. Olander, Fundamental Aspects of Nuclear Reactor Fuel Elements, TID26711-P1 (1976) 199–264.
[14] G.L. Reynolds, B. Burton, J. Nucl. Mater. 82 (1979) 22.
[15] S. Yajima, H. Furuya, T. Hirai, J. Nucl. Mater. 20 (1966) 162.